Journal of
Synchrotron Radiation

ISSN 0909-0495

Received 8 April 2004
Accepted 5 January 2005

Will reduced radiation damage occur with very small crystals?

Colin Nave[a]* and Mark A. Hill[b]

[a]CCLRC Daresbury Laboratory, Warrington WA4 4AD, UK, and [b]MRC Radiation and Genome Stability Unit, Harwell, Oxfordshire OX11 0RD, UK. E-mail: c.nave@dl.ac.uk

The primary event which occurs when an X-ray photon of energy less than 30 keV is absorbed in a protein crystal (or other organic material) is the production of a photoelectron with a similar energy to that of the absorbed photon. The electron then scatters inelastically off the surrounding material losing energy in the process. This reduction in energy takes place over track lengths of a few μm for 20 keV electrons. The vector distances between the initial and final positions of the photoelectrons are less than the track lengths owing to the non-linear tracks followed by the electrons. For crystals with smaller dimensions than the vector distances, a significant proportion of the energy could leave the crystal with the high-energy electrons. This could provide an advantage in terms of reduced radiation damage. In order to estimate the possible benefits, calculations of the electron tracks are given, initially using the continuous slowing-down approximation. A Monte Carlo approach is then used to provide more accurate values of the vector distance travelled by electrons inside a protein crystal. The calculations indicate that significant reductions in radiation damage could occur for crystals of a few μm in size. The benefits would be greater when operating at higher energies. In addition, a scheme for realising the possible benefits in a practical situation is described. This could then form the basis of trial experiments.

Keywords: radiation damage; small protein crystals.

1. Introduction

The main process which takes place when an X-ray photon of energy less than 30 keV is absorbed in organic material is the production of a high-energy photoelectron with similar energy to that of the photon. This electron then scatters elastically and inelastically off the surrounding material. The inelastic scattering results in the loss of energy of the electron which slows down after each event and eventually stops. The deposition of energy results in multiple sites of damage over a range related to the stopping distance of the electron. As the electron slows down, the stopping power increases (Fig. 1); therefore more energy is deposited towards the end of the electron track than at the beginning.

For X-ray diffraction from protein crystals, there is a desire to maximize the number of diffraction events and minimize the amount of damage. The ratio between these two processes as a function of the X-ray energy is of interest in the design of facilities for X-ray data collection from protein crystals. This has been investigated by Arndt (1984) and Nave (1995). The conclusion is that if the damage is proportional to the absorbed energy (rather than the number of photons absorbed) then the ratio will be approximately independent of the photon energy. This conclusion depends on a number of assumptions:

(i) the X-ray energies are not in the vicinity of and higher than any X-ray absorption edges;

(ii) the deposition of energy owing to Compton scattering can be ignored (Compton scattering becomes significant above 30 keV for carbon);

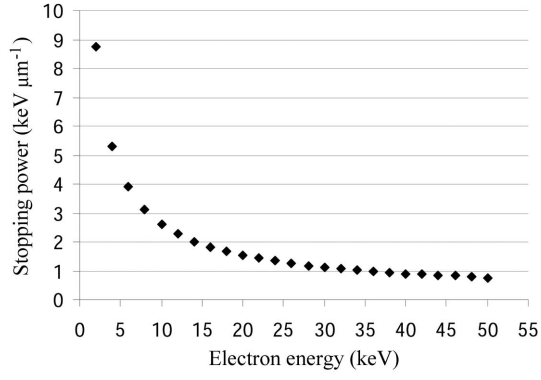

Figure 1
Electron stopping power as a function of electron energy inside a protein crystal of density 1.17 g cm^{-3}.

(iii) the X-ray transmission of the sample is high, so little information from the diffracted beams is lost;

(iv) the absorption of photoelectrons is high so all the energy deposited remains in the crystal.

This paper is mainly concerned with the last of these assumptions. If the sample (crystal plus surrounding material) is sufficiently small, the photoelectron could exit the sample, carrying a significant portion of the energy with it. In order to fully exploit this effect, it is necessary to minimize the material (*e.g.* crystal support, amorphous ice, gas) surrounding the actual crystal. Some ideas for this are included in the discussion.

There has been a considerable amount of interest in modelling electron tracks down to very low energies in the fields of microdosimetry, radiobiology and radiation chemistry (see, for example, Nikjoo *et al.*, 2002; Hill & Smith, 1993; Paretzke, 1987; Pimblott *et al.*, 1996; LaVerne & Pimblott, 1997). The subsequent chemistry of radicals produced and the biological response of mammalian cells (typical diameter size of the order of 10 μm) is very much dependent on the spatial pattern of ionizations and excitations produced along the track on the micrometre and nanometre scale.

The sizes of protein crystals being used for structure determination on high-intensity X-ray sources are becoming increasingly smaller although not yet commonly reaching the size of biological cells. It should of course be realised that the doses which are often deposited in a protein crystallography experiment (often over 10^6 Gy) far exceed those normally deposited in biological tissue during diagnostic or therapeutic medicine.

In this paper, electron path lengths in protein crystals are first estimated using concepts such as the collision stopping power and the continuous slowing-down approximation. Monte Carlo procedures are then used to derive an improved estimate for the amount of energy transmitted as the photoelectron escapes. As protein crystals vary significantly in their aspect ratio (*e.g.* cubes, needles and thin plates), the transmitted energy will depend on the direction of the photoelectron with respect to the minimum dimension of the crystal and this issue is addressed.

2. Direction of the photoelectron and sample shape

The angular distribution of the emission of photoelectrons (photoemission) depends on many factors such as the polarization of the photon (*e.g.* linear or circular), the polarization of the shell from which the electron is emitted, and orbital and spin magnetic moments of the atoms. An introduction can be found by Manson & Dill (1978), with further details by Thole & van der Laan (1994) and references therein. Most of the complexities are ignored here as we are mainly concerned with the path length of the photoelectron rather than its direction. However, the angular distribution of the photoelectron will have an effect under some circumstances.

Synchrotron radiation is strongly polarized in the horizontal direction. For a completely polarized beam and an isotropic system, the photoemission will have an angular distribution given by

$$d\sigma/d\Omega = a + b\cos^2\theta,$$

where θ is the angle from the polarization direction (Yang, 1948). Under these circumstances it would be advantageous to orient the sample so that the smallest dimensions are along the polarization direction of the X-ray beam. This would maximize the energy carried by the photoelectron escaping the sample. This might be an argument for use of more complex goniometry than the single rotation axes, normally used for protein crystallography data collection. For the present paper, this issue is not covered further. However, it should be kept in mind when designing experiments to test any reduction in radiation damage.

3. Path lengths of photoelectrons in water and other material

The path length of photoelectrons depends on the energy of the photoelectron, the composition of the material, the density of the material and, as a further complication, the structure of the material. This last complication is ignored here although it has been pointed out that, owing to changes in dielectric strength, path lengths of electrons in crystalline material can be significantly longer than in a disordered structure (Tanaka *et al.*, 1991).

A simple analysis of the path lengths of photoelectrons can be derived from concepts such as the continuous slowing-down range and the collision stopping power. The collision stopping power is the average rate of energy loss per unit path length, owing to Coulomb collisions that result in the ionization and excitation of atoms. The radiative stopping power, which involves bremstrahlung radiation owing to collisions of these electrons with atoms and electrons, can be ignored at the photon energies considered here. The continuous slowing-down approximation assumes that the rate of energy loss at each point along the track is equal to the stopping power for the photoelectron at that point. From this, the range of the particle (the continuous slowing-down approximation range or CSDA range) can be calculated.

In order to calculate these parameters the atomic composition and density of the protein crystal are required.

The atomic composition used is given below (taken from an example given for a bio-informatics toolkit at http://www.mathworks.com/access/helpdesk/help/toolbox/bioinfo/a1048187091.html with atoms for 1856 molecules of water added):

C: 1818; H: 7286; N: 420; O: 2673; S: 25.

This corresponds to a 50% solvent content. The average partial specific volume of a protein in a crystal is 0.74 $cm^3\ g^{-1}$ (Matthews, 1968). This gives a density for the crystal of 1.17 $g\ cm^{-3}$.

Plots of the stopping power and CSDA range as a function of electron energy are shown in Figs. 1 and 2. These were calculated using the program *estar* (Berger *et al.*, 2000). This

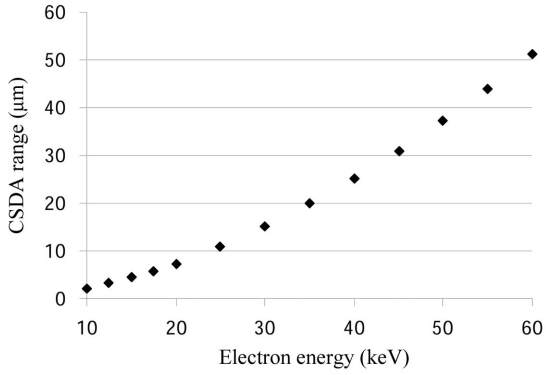

Figure 2
Range of electrons inside a large protein crystal calculated using the continuous slowing-down approximation (CSDA).

program uses mean excitation energies (*I* values) (ICRU, 1984). Similar values for electron ranges are given by Paretzke (1987), Blohm (1983) and Pimblott *et al.* (1996) for calculations in water. [Note that there is an error in Pimblott *et al.* (1996): the ranges given in Tables 2 and 3 are a factor of ten too large (Pimblott, personal communication)]. The uncertainties of the calculated collision stopping powers for electrons are estimated (ICRU, 1984) to be 1–2% above 100 keV, 2–3% (in low-*Z* materials) and 5–10% (in high-*Z* materials) between 100 and 10 keV and of the order of 10% for low-*Z* materials at 1 keV. The increasing uncertainties at low energies are due to the lack of shell corrections which are required when the velocity of the incident electron is no longer large compared with the velocities of the atomic electrons, especially those in the inner shells. These limitations do not significantly affect the results of the calculations presented here.

From the stopping-power values it is possible to calculate the distance travelled by an electron after a certain loss in energy. For example, a 40 keV electron will lose approximately 10 keV in a distance of 10 μm inside a protein crystal. A 20 keV electron would lose this energy in a path length of approximately 5 μm. However, this represents the distance travelled by an electron along its path rather than the distance from its origin. The electron path is non-linear owing to both inelastic and elastic scattering events (LaVerne & Pimblott, 1997). It is not possible to provide a simple correction to take account of this, as the ratio between the vector distance and the path travelled varies as the electron loses energy.

The approach above therefore only gives a rough estimate of the amount of energy likely to be deposited and transmitted when a high-energy electron is created owing to X-ray absorption. The program *CASINO* (Hovington *et al.*, 1997) was therefore used to provide a more complete description of the electron track structure and the amount of energy carried out of the sample by photoelectrons which emerge from it.

An example of the tracks of 30 keV photoelectrons derived from *CASINO* is given in Fig. 3. When the transmission is high, the majority (over 85% in Fig. 3) of photoelectrons emerge from the sample in a direction close to their initial direction. They have a distribution of energies dependent on the number and strength of the inelastic collisions each electron has undergone. Examples of such distributions are given in Fig. 4. By summing these distributions, values for the energy which escapes the sample can be obtained. These are given in Table 1. The numbers show that a significant proportion of the energy could escape a crystal of a few μm in size when operating at photon energies above 20 keV. As an example, a crystal of 8 μm dimensions and a 30 keV X-ray beam are considered. Photoelectrons emitted 8 μm from the exit surface will on average deposit 63% of their energy in the crystal. Those emitted at 4 μm from the exit will deposit 24% of their energy and those emitted at the surface will deposit negligible energy. A total gain, in diffraction dose efficiency (Murray *et al.*, 2004), *i.e.* diffracted photons per absorbed dose, of approximately a factor of 3 could therefore occur under these

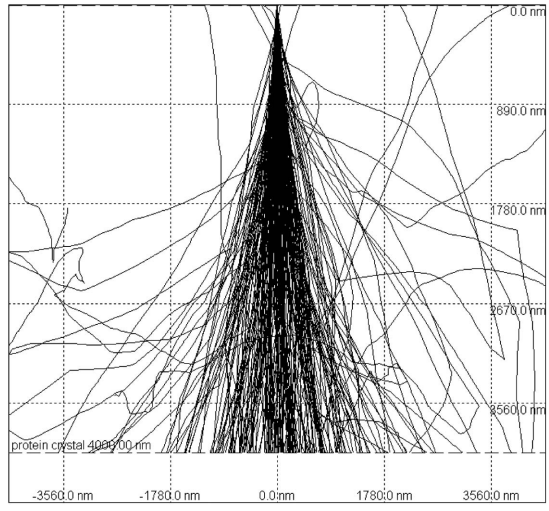

Figure 3
A simulation of tracks, created by electrons of 30 keV energy produced in the centre of an 8 μm-sized protein crystal, calculated using the Monte Carlo program *CASINO*. Most of the electrons emerge from the face of the crystal 4 μm from the initial position of the electron (corresponding to the site of X-ray absorption).

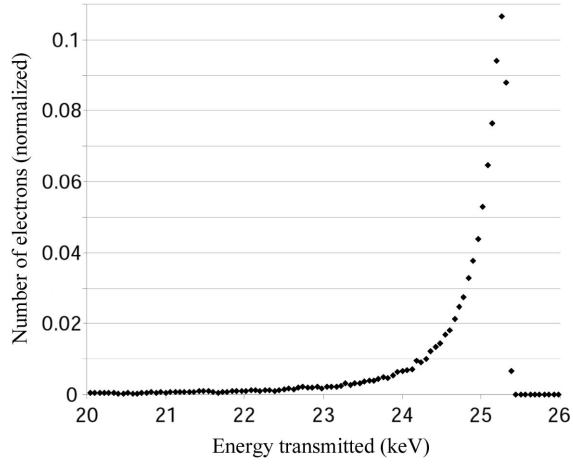

Figure 4
Spectrum of electron energies emerging from the face of a protein crystal 4 μm away from the source of production of 30 keV photoelectrons. Integration under these curves gives the transmitted energy (see Table 1).

Table 1
Percentage of energy which escapes from a sample as a function of the initial energy of the photoelectron and its initial distance from the surface.

The normal to the surface is assumed to be along the initial direction of the photoelectron and only electrons which emerge from this surface are included. This slightly underestimates the total transmission for an electron originating in the centre of a cube-shaped crystal (see, for example, Fig. 3).

	Transmitted energy (%) at given initial energy			
Distance from surface (μm)	10 keV	20 keV	30 keV	40 keV
0.5	79	95		
1	23	89		
2	0	74	90	94
4		34	76	87
8		0	37	57
16			0	23
32				0

circumstances. This should be a reasonable estimate of the benefit which could occur. The estimate ignores the energy deposition owing to Compton scattering. This becomes increasingly important for X-ray energies above 20 keV, with a cross section comparable with that for photoelectric absorption. Only a fraction of the energy of the incident X-ray is transferred to the Compton electron (for example, the mean energy of the emitted Compton electron is only 1.56 keV for a 30 keV X-ray). The electron will therefore have a very short range and deposit almost all its energy in the crystal. However, this is only about 5% of the total energy of the X-ray photon. Ignoring the Compton scattering will underestimate the radiation damage, while ignoring electrons which escape at a large angle to their initial direction will overestimate it (by up to 15% in the example shown here). The approximations made here are therefore unlikely to affect the conclusions significantly. In order to progress the simulations further, the calculations will have to be carried out for all crystal orientations, photoelectron origins and photoelectron directions with the contribution of Compton scattering included. The simulations are best considered as applying to the sample as a whole (crystal plus surrounding support and amorphous ice).

4. Discussion

The energy deposited is determined by the spatial pattern of radiation tracks and is independent of dose rate. Radiation traverses a typical protein molecule of dimensions a few nm in 10^{-17} s, the energy transfer (ionization and excitation events) takes place over 10^{-17}–10^{-16} s, with typical lifetimes of 10^{-15}–10^{-14} s, and the thermalization of electrons occurs on timescales of $\sim 10^{-13}$ s (see, for example, Klassen, 1987). For longer timescales, any dose-rate effect will depend on radical lifetimes and diffusion distances. At these high doses, the radicals produced along individual tracks are likely to be in close proximity. They may interact if the radicals from the first track are still present when the radicals from the second track are produced. However, with irradiation while the sample is held at the usual cryo-temperature of 100 K in a stream of gaseous nitrogen, the diffusion of radicals will be minimized, resulting in the direct effect dominating (O'Neill *et al.*, 2002).

In order to realise reduced radiation damage when electrons escape the sample, it is necessary to minimize the amount of surrounding material which, if illuminated with X-rays, could feed energy into the sample. In addition, it is desirable to ensure that electrons which leave the sample truly escape rather than return to the sample (this might occur if the sample becomes positively charged). A sample-mounting method similar to that used in electron microscopy might be appropriate. This could involve a thin carbon film supported on an electron microscope grid. Holes in the film would be occupied by a thin layer of amorphous ice containing the crystals to be examined. Additional carbon coating might be necessary to reduce charge build-up on the specimen. Similar arrangements with lacey supports could be attempted. For helium, the cross sections for both Rayleigh scattering and photoabsorption are much less than for air. A helium flow at 100 K will therefore minimize creation of photoelectrons outside the sample as well as reduce X-ray background. An X-ray beam could be scanned across the sample, collecting data for crystals in random orientations as they are illuminated by the beam. It would be necessary to assemble a complete data set from noisy and incomplete data obtained from each crystal. Similar procedures are becoming common in electron microscopy.

Such a set-up could provide advantages in reducing radiation damage irrespective of any benefits owing to reduced energy deposition. By ensuring minimum path length for the surrounding material, a lower X-ray background will be obtained for the small crystals considered here, where background from sources other than the sample would otherwise dominate. This should make it possible to maximize the information obtained from each protein crystal before the crystal suffers radiation damage.

Optimization of the experimental set-up could give a 'window' of crystal sizes between those amenable to electron diffraction (typically less than 0.1 μm thickness) and larger crystals (where photoelectrons are totally absorbed). For crystals with larger unit cells, a multiple crystal approach, as commonly used for data collection from virus crystals, would have to be adopted. Several authors have estimated the minimum crystal size for which it should be possible to collect a single diffraction image, with an incident dose which will still retain reasonable diffraction. For example, a figure of 8 μm in each dimension for a typical protein crystal was quoted by Teng & Moffat (2002). Using higher-energy radiation it should be possible to collect approximately three times as many images from a single crystal of this size. Alternatively, it should be possible to use a crystal of 4 μm in each dimension to collect one image. Although this would require eight times the X-ray exposure, owing to the smaller volume, approximately 7/8 of the energy would escape the crystal. Regarding the dependence of exposure time on wavelength, for the same number of incident X-ray photons this varies with $1/\lambda^2$ (see, for example, Arndt, 1984). However, with modern third-generation synchrotron sources this should not be a problem.

A detector with adequate efficiency at these shorter wavelengths would need to be available, as any gains owing to decreased radiation damage could easily be lost owing to detector inefficiency. The main problem with carrying out tests is that high-energy radiation will be required to realise the potential benefits for crystals more than a few μm in size. The majority of present and planned protein crystallography beamlines, including those capable of producing focused beams of a few μm in size, are optimized (in terms of the X-ray source, optics and detectors) for energies under 20 keV where significant benefit will only occur for crystals less than 4 μm in size.

Edgar Weckert and Gerrit van der Laan are thanked for useful discussions concerning the angular distribution of photoelectrons. Richard Henderson is thanked for alerting one of the authors (CN) to the issue of electron ranges in protein crystals.

References

Arndt, U. W. (1984). *J. Appl. Cryst.* **17**, 118–119.
Berger, M. J., Coursey, J. S. & Zucker, M. A. (2000). *ESTAR, PSTAR and ASTAR: Computer Programs for Calculating Stopping Power and Range Tables for Electrons, Protons and Helium Ions.* Version 1.2.2. National Institute of Standards and Technology, Gaithersburg, MD, USA. (Available online at http://physics.nist.gov/Star.)
Blohm, R. (1983). Dissertation, Universität Göttingen, Germany.
Hill, M. A. & Smith, F. A. (1993). *Radiat. Phys. Chem.* **43**, 265–280.
Hovington, P., Drouin, D. & Gauvin, R. (1997). *Scanning*, **19**, 1–14. (See http://www.gel.usherb.ca/casino/index.html.)
ICRU (1984). *Stopping Powers for Electrons and Positrons*, ICRU Report 37. International Commission on Radiation Units and Measurements, 7910 Woodmont Avenue, Suite 400, Bethesda, MD 20814-3095, USA.
Klassen, N. V. (1987). *Radiation Chemistry Principles and Applications*, edited by Farhataziz and M. A. J. Rogers, pp. 29–64. New York: VCH.
LaVerne, J. A. & Pimblott, S. M. (1997). *J. Phys. Chem. A*, **101**, 4504–4510.
Manson, S. T. & Dill, D. (1978). *Electron Spectroscopy: Theory, Techniques and Applications*, Vol. 2, edited by C. R. Brundle and A. D. Wilson. New York: Academic Press.
Matthews, B. W. (1968). *J. Mol. Biol.* **33**, 491–497.
Murray, J. W., Garman, E. F. & Ravelli, R. B. G. (2004). *J. Appl. Cryst.* **37**, 513–522.
Nave, C. (1995). *Radiat. Phys. Chem.* **45**, 483–490.
Nikjoo, H., Bolton, C. E., Watanabe, R., Terrissol, M., O'Neill, P. & Goodhead, D. T. (2002). *Radiat. Prot. Dosim.* **99**, 77–80.
O'Neill, P., Stevens, D. L. & Garman, E. F. (2002). *J. Synchrotron Rad.* **9**, 329–332.
Paretzke, H. G. (1987). In *Kinetics on Nonhomogeneous Processes*, edited by G. R. Freeman. New York: Wiley.
Pimblott, S. A., LaVerne, J. A. & Mozumder, A. (1996). *J. Phys. Chem.* **100**, 8595–8606.
Tanaka, Y., Ohnuma, N., Katsunami, K. & Ohki, Y. (1991). *IEEE Trans. Electr. Insul.* **26**, 258–265.
Teng, T.-Y. & Moffat, K. (2002). *J. Synchrotron Rad.* **9**, 198–201.
Thole, B. T. & van der Laan, G. (1994). *Phys. Rev. B*, **49**, 9613–9631.
Yang, C. N. (1948). *Phys. Rev.* **74**, 764.